# Effects of Anisotropic Thermal Conductivity in Magnetohydrodynamics Simulations of a Reversed-Field Pinch

M. Onofri, F. Malara, and P. Veltri

*Dipartimento di Fisica, Università della Calabria, ponte Bucci, Cubo 31C, 87036 Rende (CS), Italy*

(Received 13 July 2010; published 17 November 2010)

A compressible magnetohydrodynamics simulation of the reversed-field pinch is performed including anisotropic thermal conductivity. When the thermal conductivity is much larger in the direction parallel to the magnetic field than in the perpendicular direction, magnetic field lines become isothermal. As a consequence, as long as magnetic surfaces exist, a temperature distribution is observed displaying a hotter confined region, while an almost uniform temperature is produced when the magnetic field lines become chaotic. To include this effect in the numerical simulation, we use a multiple-time-scale analysis, which allows us to reproduce the effect of a large parallel thermal conductivity. The resulting temperature distribution is related to the existence of closed magnetic surfaces, as observed in experiments. The magnetic field is also affected by the presence of an anisotropic thermal conductivity.

DOI: 10.1103/PhysRevLett.105.215006 PACS numbers: 52.55.Hc

A reversed-field pinch (RFP) is a toroidal configuration for magnetic confinement of fusion plasmas. Differently from the tokamak, most of the magnetic field is generated by currents flowing in the plasma, through a dynamo effect produced by magnetohydrodynamic (MHD) instabilities [1–3]. In the past, a broad spectrum of instabilities was considered necessary for the sustainment of the configuration. Such instabilities are also responsible for a stochastization of the magnetic field, due to the superposition of many unstable modes. This kind of configuration, where many MHD modes of comparable amplitudes are present, are called multiple helicity (MH) states. The magnetic chaos characterizing MH states is a problem for energy confinement. However, it has been shown that, in principle, the RFP can also be obtained with a dynamo effect produced by a single mode [4]. In such a configuration, called single helicity (SH) state, the magnetic field is not chaotic and conserved magnetic surfaces exist. In recent years, quasisingle helicity (QSH) states, where a dominant mode exists together with small amplitude secondary modes, have been observed in different machines [5–9] and numerical simulations [10]. QSH states have been observed to appear spontaneously, alternating with MH states. Experiments show that the persistence of QSH states increases with the Lundquist number and plasma current [11]. Two classes of QSH states have been observed in experiments. In the first case, there is a magnetic island with a separatrix and two magnetic axes, the original magnetic axis and a helical magnetic axis corresponding to the island $O$ point. The second class of QSH states is formed when the dominant mode grows above a certain threshold, the separatrix and the original magnetic axis disappear, and a single helical magnetic axis remains [11]. This second class of QSH states has been named single helical axis and they have improved confinement properties.

The possibility of obtaining QSH states is important in order to achieve better confinement properties. In MH states the temperature is almost flat in the plasma core, while in QSH states strong temperature gradients appear and a hot structure is formed in coincidence with the magnetic island, indicating that a better thermal confinement is obtained in the magnetic island [11,12]. A reduction of energy and particle transport has been observed in QSH states with respect to MH states [13–15]. The different behavior of temperature in MH states and in QSH states is due to the strong anisotropy of the thermal conductivity. In fact, the thermal conductivity in a magnetized plasma is anisotropic with respect to the direction of the magnetic field, and in a fusion plasma the ratio $\kappa_\parallel/\kappa_\perp$ may exceed $10^{10}$ [16] ($\kappa_\parallel$ and $\kappa_\perp$ are the parallel and perpendicular thermal conductivities). While in the perpendicular direction the thermal conductivity is very small, in the parallel direction it has the effect of making magnetic field lines isothermal. As a consequence, in MH states, where the magnetic field is chaotic, the radial heat transport is more efficient than in QSH states, where well conserved magnetic surfaces exist.

Numerical MHD simulations of the RFP were usually performed with the assumptions of constant density and pressure, so that a description of temperature was not available [10,17]. Some progress in the numerical study of the RFP has been made including density and pressure dynamics [18–20]. Indeed, a self-consistent treatment of density and pressure dynamics gives better control of the physics involved in the RFP evolution. However, a realistic value of the parallel thermal conductivity in the energy equation would introduce a time scale much shorter than the other typical time scales characterizing the system evolution. The resolution of such a short time scale would require an extremely small time step and the simulation would be out of the possibilities of any computing system. For this reason, up to now, simulations using explicit time

 

schemes were performed either with vanishing thermal conductivity or with an isotropic thermal conductivity ($\kappa_\parallel = \kappa_\perp$). On the contrary, in this Letter we have set up a new numerical technique which allows us to solve MHD compressible equations when $\kappa_\parallel \gg \kappa_\perp$. We show that the different behavior of temperature observed in QSH and MH states can be reproduced in numerical simulations including an anisotropic thermal conductivity.

We solve the compressible MHD equations in cylindrical coordinates $(r, \theta, z)$, in dimensionless form [19–21], writing the heat flux in the form

$$\mathbf{q} = \kappa_\parallel \boldsymbol{\nabla}_\parallel T + \kappa_\perp \boldsymbol{\nabla}_\perp T. \tag{1}$$

The magnetic field and density are normalized to typical values $B_0$ and $\rho_0$, respectively. The radius $a$ of the cylinder is used as unit length scale and time is normalized to the typical Alfvén time $\tau_A = a/v_A$, where $v_A = B_0/\sqrt{4\pi\rho_0}$ is the Alfvén velocity. Finally, the pressure $p$ is measured in units of $\rho_0 v_A^2$ and the temperature is $T = p/\rho$. The numerical code uses a pseudospectral method in the periodic directions ($\theta$ and $z$), compact differences in the radial direction, and an explicit Runge-Kutta time scheme.

Boundary conditions are imposed assuming that the plasma is bounded by a rigid wall acting as a perfect conductor [19], with constant temperature. No-slip boundary conditions are imposed on velocity. The current density $J_\theta$ and $J_z$ vanish at the conducting boundary, except for the $m = 0$, $n = 0$ mode ($m$ and $n$ are the poloidal and toroidal mode numbers, respectively). For the $(0, 0)$ mode we impose constant poloidal magnetic field at the boundary, which corresponds to a constant toroidal current, and constant toroidal magnetic field, which is obtained with the external toroidal field coils. A time dependent boundary condition for density is derived using a characteristic wave decomposition [22]. It is described in detail in Ref. [21] and it corresponds to the reflection of fast magnetosonic waves at the walls. The set of boundary conditions used in this simulation is different from that used in [20], because we impose a constant toroidal magnetic field for the $(0, 0)$ mode instead of constant toroidal flux. The condition used in this Letter is closer to experimental conditions, where the toroidal magnetic field at the edge is directly determined by the external coils [3].

As the initial state, a force-free equilibrium magnetic field has been chosen [20]. The initial density and pressure are uniform, with $\rho = 1$ and $p = 0.05$.

To overcome the difficulty of using a realistic value of $\kappa_\parallel$ we perform a multiple-time-scale analysis [23] of the MHD compressible equations. In particular, we consider that the evolution equation for pressure $p$ contains a term $\kappa_\parallel \boldsymbol{\nabla}_\parallel T$ which can be associated with a time scale much shorter than all other terms. Therefore, we can write the equation in the following form:

$$\frac{\partial p}{\partial t} = -\epsilon[\boldsymbol{\nabla}\cdot(\mathbf{v}p - \kappa_\perp \boldsymbol{\nabla}_\perp T) + (\gamma - 1)p\boldsymbol{\nabla}\cdot\mathbf{v}] + \epsilon(\gamma - 1)H_p + \boldsymbol{\nabla}\cdot(\kappa_\parallel \boldsymbol{\nabla}_\parallel T), \tag{2}$$

with $\epsilon \ll 1$ and $H_p$ is the heat production due to viscosity and resistivity. We expand $p$ in the small parameter $\epsilon$

$$p \simeq p_0 + \epsilon p_1 + \epsilon^2 p_2 + \cdots. \tag{3}$$

Moreover, we introduce new time variables $\tau_0, \tau_1, \tau_2, \ldots$, such that

$$\frac{d\tau_0}{dt} = 1, \quad \frac{d\tau_1}{dt} = \epsilon, \quad \frac{d\tau_2}{dt} = \epsilon^2, \ldots. \tag{4}$$

The freedom introduced by extending the number of time variables can be used to remove the time secularities in the solution. This allows us to separate fast time scales from slow time scales, and to obtain the equations

$$\frac{\partial p_0}{\partial \tau_0} = \boldsymbol{\nabla}\cdot\left[\kappa_\parallel \boldsymbol{\nabla}_\parallel\left(\frac{p_0}{\rho}\right)\right], \tag{5}$$

$$\frac{\partial p_0}{\partial \tau_1} = -\left[\boldsymbol{\nabla}\cdot\left(\mathbf{v}p_0 - \kappa_\perp \boldsymbol{\nabla}_\perp \frac{p_0}{\rho}\right) + (\gamma - 1)p_0\boldsymbol{\nabla}\cdot\mathbf{v}\right] + (\gamma - 1)H_p. \tag{6}$$

The other equations that must be solved are of order $\epsilon^1$; i.e., they evolve on the time scale $\tau_1$. After each time step $\Delta\tau_1$ we solve numerically Eq. (5) until $p_0$ reaches an asymptotic value. It is worth noting that, due to the fact that $\kappa_\parallel \gg \kappa_\perp$, we do not need to use in Eq. (5) the exact value of the physical parallel thermal conductivity, but only a numerical parameter that determines the time needed to find an asymptotic stationary solution for $p_0$. The solution of Eq. (5) has the effect of producing isothermal magnetic field lines and the result is independent of the specific value of $\kappa_\parallel$, which has been chosen $\kappa_\parallel = 1$. Then we substitute $p_0$ in Eq. (6) and in the other equations that must be solved and perform the subsequent time step $\Delta\tau_1$.

The simulation has been carried out with the following parameters:

$$\eta = 10^{-3}, \qquad \mu = 10^{-3}, \qquad \kappa_\perp = 10^{-3}, \tag{7}$$

$$R = 4, \qquad q(0) = 0.1, \tag{8}$$

where $\eta$ and $\mu$ are the dimensionless resistivity and viscosity, respectively, $R$ is the aspect ratio, and $q(0)$ is the on-axis safety factor. We perturbed the initial equilibrium by exciting a few modes close to the most unstable one.

In Fig. 1 we plot the time evolution of the reversal parameter $F = B_z^{(0,0)}(a)/\langle B_z\rangle$, where $B_z^{(0,0)}(a)$ is the $(0, 0)$ mode amplitude of the toroidal field at the boundary and $\langle B_z\rangle$ is the average of $B_z^{(0,0)}$ over a poloidal cross section. In the beginning, the resistive diffusion makes the toroidal flux decrease, causing a decrease of $F$. After $t \simeq 500$ a stationary state is reached where an equilibrium is obtained

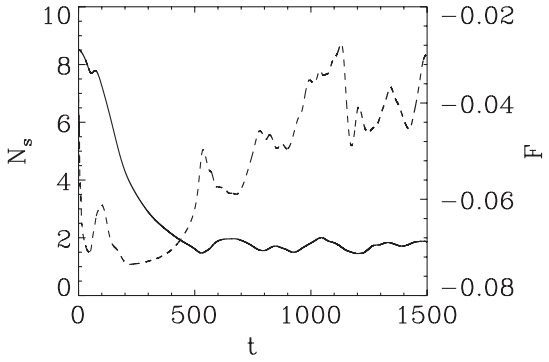


FIG. 1. Time evolution of the reversal parameter $F$ (solid line) and of the spectral spread $N_s$ (dashed line) in the simulation with anisotropic thermal conductivity.

between dissipation and the dynamo effect produced by the unstable modes. Since the boundary conditions impose that the toroidal and poloidal fields at the edge are constant in time, the evolution of the toroidal flux and of the pinch parameter $\Theta = B_\theta^{(0,0)}(a)/\langle B_z \rangle$ are only determined by the evolution of the reversal parameter. The toroidal flux is inversely proportional to $F$, while $\Theta$ is proportional to $F$. To show the transition between MH and SH states, the spectral index $N_s$ has been plotted in Fig. 1. As usual, the parameter $N_s$ is defined as [24]

$$N_s^{-1} = \sum_n \left( \frac{B_{1,n}^2}{\sum_n B_{1,n}^2} \right)^2, \tag{9}$$

where

$$B_{1,n}^2 = \int_0^1 |B_{1,n}|^2 r dr. \tag{10}$$

The parameter $N_s$ is equal to 1 in SH states. Figure 1 shows many oscillations in the evolution of $N_s$, which indicates the presence of QSH states at $t \simeq 50$ and in the interval between $t \simeq 200$ and $t \simeq 400$.

In Figs. 2 and 3 we show temperature contours and Poincaré plots of the magnetic field in the plane $z = 0$ in a QSH state and in a MH state. At $t = 260$ the system is in

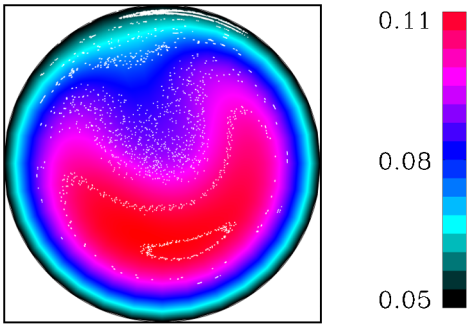


FIG. 2 (color online). Poincaré maps of the magnetic field (white dots) and contours of temperature in the plane $z = 0$ at $t = 260$. Simulation with anisotropic thermal conductivity.

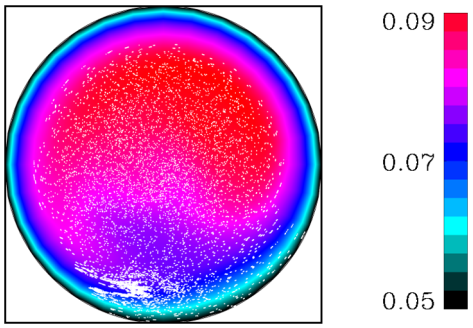


FIG. 3 (color online). Poincaré maps of the magnetic field (white dots) and contours of temperature in the plane $z = 0$ at $t = 1000$. Simulation with anisotropic thermal conductivity.

a QSH state and a dominant $m = 1$, $n = -8$ mode is visible in the temperature distribution. A hot island is present corresponding to the magnetic field bean-shaped region. A chaotic region is visible, but magnetic surfaces also exist and magnetic field lines do not connect the hot bean-shaped region in the core with the cold region near the boundary. On the other hand, in the MH state at $t = 1000$ the magnetic field is completely chaotic and the large parallel heat transport makes the temperature much more uniform. As expected, magnetic field lines are almost isothermal. This is also visible in Fig. 4, where a temperature profile is plotted along a diameter at $\theta = \pi/2$ and $z = 0$. At $t = 260$ the temperature profile shows the presence of a hot island, while at $t = 1000$ it becomes almost flat in the central region. Notwithstanding the initial uniform density profile, at later times density becomes spatially modulated, with low values corresponding to the hotter region, and finally in the stationary state it shows an almost flat central region, decreasing near the wall.

For comparison, a second simulation has been performed with the same parameters and the same boundary conditions, but with isotropic thermal conductivity $\kappa = 10^{-3}$. In Figs. 5 we show temperature contours and Poincaré plots of the magnetic field in the plane $z = 0$ at

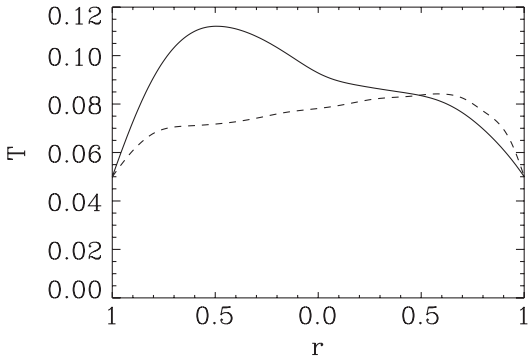


FIG. 4. Temperature profiles along the diameter $\theta = \pi/2$ and $z = 0$ at $t = 260$ (solid line) and $t = 1000$ (dashed line). Simulation with anisotropic thermal conductivity.

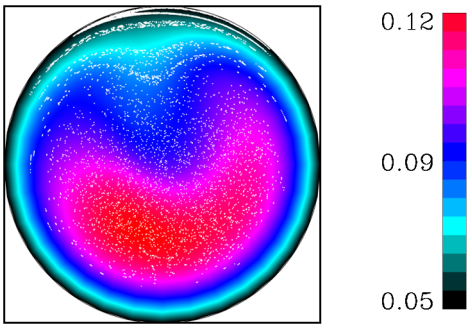


FIG. 5 (color online). Poincaré maps of the magnetic field (white dots) and contours of temperature in the plane $z = 0$ at $t = 260$. Simulation with isotropic thermal conductivity.

$t = 260$. At this time the spectral index $N_s$ is close to 1 and a dominant $m = 1$, $n = -8$ mode is visible in the temperature distribution, but the presence of a $m = 2$ mode with amplitude comparable to the dominant mode makes the magnetic field chaotic, except in the outer region, where some magnetic surfaces are visible. In Fig. 5 a hot island is still present, even though the magnetic field is chaotic. At $t = 1000$, magnetic surfaces are also destroyed in the outer region, but the temperature contours show the existence of a hot bean-shaped structure in the poloidal plane. It is worth noting that the presence of an anisotropic thermal conductivity does not only modify the temperature distribution, but it also has important dynamical effects on the magnetic field evolution. In fact, the magnetic field shown in Fig. 2 is significantly different from that obtained with an isotropic thermal conductivity (Fig. 5). These results are different from those described in [20], where different boundary conditions were used. In that case, constant toroidal flux was imposed, while in the present simulation this condition has been replaced by a constant toroidal field for the $(0, 0)$ mode at the edge. In the simulation presented in [20], a stationary state with negative $F$ was not obtained and the evolution of the spectral index $N_s$ indicated the existence of a QSH state between $t \simeq 50$ and $t \simeq 150$.

The results obtained with anisotropic thermal conductivity show a good correspondence of temperature contours with magnetic field lines and are similar to experimental observations, where there is a relation between the temperature distribution and the magnetic field topology. In QSH states large temperature gradients are produced, with the formation of a hot bean-shaped island, while in MH states the temperature becomes almost flat. Our results show that the temperature behavior observed in QSH and MH states can be produced as the effect of an anisotropic thermal conductivity. This is a key ingredient that should be included in simulations in order to reproduce a realistic evolution of the system.

[1] D. D. Schnack and S. Ortolani, Nucl. Fusion **30**, 277 (1990).
[2] S. Ortolani and D. D. Schnack, *Magnetohydrodynamics of Plasma Relaxation* (World Scientific, Singapore, 1993).
[3] P. Martin *et al.*, Plasma Phys. Controlled Fusion **49**, A177 (2007).
[4] J. M. Finn, R. A. Nebel, and C. Bathke, Phys. Fluids B **4**, 1262 (1992).
[5] P. Martin *et al.*, Nucl. Fusion **43**, 1855 (2003).
[6] D. F. Escande *et al.*, Phys. Rev. Lett. **85**, 1662 (2000).
[7] P. Nordlund and S. Mazur, Phys. Plasmas **1**, 4032 (1994).
[8] P. Brunsell *et al.*, Phys. Fluids B **5**, 885 (1993).
[9] J. S. Sarff, N. E. Lanier, S. C. Prager, and M. R. Stoneking, Phys. Rev. Lett. **78**, 62 (1997).
[10] S. Cappello and D. F. Escande, Phys. Rev. Lett. **85**, 3838 (2000).
[11] R. Lorenzini *et al.*, Nature Phys. **5**, 570 (2009).
[12] R. Lorenzini *et al.*, Phys. Rev. Lett. **101**, 025005 (2008).
[13] L. Frassinetti, P. R. Brunsell, and J. Drake, Phys. Plasmas **16**, 032503 (2009).
[14] I. Predebon, L. Marrelli, R. B. White, and P. Martin, Phys. Rev. Lett. **93**, 145001 (2004).
[15] M. Gobbin, L. Marrelli, and R. B. White, Plasma Phys. Controlled Fusion **51**, 065010 (2009).
[16] R. Fitzpatrick, Phys. Plasmas **2**, 825 (1995).
[17] S. Cappello, D. Biskamp, Nucl. Fusion **36**, 571 (1996).
[18] M. Onofri, F. Malara, and P. Veltri, Phys. Rev. Lett. **101**, 255002 (2008).
[19] M. Onofri, F. Malara, and P. Veltri, Phys. Plasmas **16**, 052508 (2009).
[20] M. Onofri, F. Malara, and P. Veltri, Nucl. Fusion **50**, 055003 (2010).
[21] M. Onofri, L. Primavera, F. Malara, and P. Londrillo, J. Comput. Phys. **226**, 1874 (2007).
[22] T. J. Poinsot and S. K. Lele, J. Comput. Phys. **101**, 104 (1992).
[23] R. C. Davidson, *Methods in Nonlinear Plasma Theory* (Academic, New York, 1972).
[24] L. Frassinetti, I. Predebon, H. Koguchi, Y. Yagi, Y. Hirano, H. Sakakita, G. Spizzo, and R. B. White, Phys. Rev. Lett. **97**, 175001 (2006).